

Investigation of the isoscalar response of  $^{24}\text{Mg}$  to  $^6\text{Li}$  scattering

J. C. Zamora <sup>1</sup>, C. Sullivan,<sup>2,3,4</sup> R. G. T. Zegers,<sup>2,3,4</sup> N. Aoi,<sup>5</sup> L. Batail,<sup>6,7</sup> D. Bazin,<sup>2,4</sup> M. Carpenter,<sup>8</sup> J. J. Carroll,<sup>9</sup> Y. D. Fang,<sup>5</sup> H. Fujita,<sup>5</sup> U. Garg,<sup>10</sup> G. Gey,<sup>5</sup> C. J. Guess,<sup>11,\*</sup> M. N. Harakeh,<sup>5,12</sup> T. H. Hoang,<sup>5</sup> E. Hudson,<sup>11,†</sup> N. Ichige,<sup>13</sup> E. Ideguchi,<sup>5</sup> A. Inoue,<sup>5</sup> J. Isaak,<sup>5,14</sup> C. Iwamoto,<sup>15</sup> C. Kacir,<sup>11,‡</sup> N. Kobayashi,<sup>5</sup> T. Koike,<sup>13</sup> M. Kumar Raju,<sup>5</sup> S. Lipschutz,<sup>2,3,4</sup> M. Liu,<sup>16</sup> P. von Neumann-Cosel,<sup>14</sup> S. Noji,<sup>2,3</sup> H. J. Ong,<sup>5,§</sup> S. Péru,<sup>6,7</sup> J. Pereira,<sup>2,3</sup> J. Schmitt,<sup>2,3,4</sup> A. Tamii,<sup>5</sup> R. Titus,<sup>2,3,4</sup> V. Werner,<sup>14</sup> Y. Yamamoto,<sup>5</sup> X. Zhou,<sup>16</sup> and S. Zhu<sup>8</sup>

<sup>1</sup>*Instituto de Física, Universidade de Sao Paulo, SP 05508-090, Brazil*

<sup>2</sup>*National Superconducting Cyclotron Laboratory, Michigan State University, East Lansing, Michigan 48824, USA*

<sup>3</sup>*Joint Institute for Nuclear Astrophysics, CEE, Michigan State University, East Lansing, Michigan 48824, USA*

<sup>4</sup>*Department of Physics and Astronomy, Michigan State University, East Lansing, Michigan 48824, USA*

<sup>5</sup>*Research Center for Nuclear Physics (RCNP), Osaka University, Ibaraki, Osaka 567-0047, Japan*

<sup>6</sup>*CEA, DAM, DIF, F-91297 Arpajon, France*

<sup>7</sup>*Université Paris-Saclay, CEA, LMCE, 91680 Bruyères-le-Châtel, France*

<sup>8</sup>*Argonne National Laboratory, Argonne, Illinois 60439, USA*

<sup>9</sup>*DEVCOM/Army Research Laboratory, Adelphi, Maryland 20783, USA*

<sup>10</sup>*Department of Physics, University of Notre Dame, Notre Dame, Indiana 46556, USA*

<sup>11</sup>*Department of Physics and Astronomy, Swarthmore College, Swarthmore, Pennsylvania 19081, USA*

<sup>12</sup>*Nuclear Energy group, ESRIG, University of Groningen, 9747 AA Groningen, The Netherlands*

<sup>13</sup>*Department of Physics, Tohoku University, Sendai 980-8578, Japan*

<sup>14</sup>*Institute for Nuclear Physics, Technical University Darmstadt, D-64289 Darmstadt, Germany*

<sup>15</sup>*Center for Nuclear Study, University of Tokyo (CNS) RIKEN Campus, 2-1 Hirosawa, Wako, Saitama 351-0198, Japan*

<sup>16</sup>*Institute of Modern Physics, Chinese Academy of Sciences, Lanzhou, China*



(Received 17 May 2021; accepted 24 June 2021; published 7 July 2021)

**Background:**  $^{24}\text{Mg}$  is a strongly deformed nucleus in the ground state. Deformation effects can be observed in the structure of the isoscalar giant monopole and quadrupole resonances.  $^{24}\text{Mg}$  is also a nucleus that is well known to present different types of cluster-oscillation modes. Both giant resonances and cluster states are strongly populated by isoscalar transitions.

**Purpose:** To extract the  $E0$ ,  $E1$ , and  $E2$  transition strengths via  $^6\text{Li}$  scattering. The  $^6\text{Li}$  probe is a powerful tool for investigating the isoscalar nuclear response with a very favorable ratio of resonance-to-continuum background.

**Method:** Double-differential cross sections of  $^6\text{Li}$  inelastic scattering, at the beam energy of 100 MeV/u, were measured in the excitation-energy range 10–40 MeV and scattering angles  $0\text{--}3^\circ$ . A multipole-decomposition analysis was performed for extracting the isoscalar  $E0$ ,  $E1$ , and  $E2$  strength distributions.

**Results:** The extracted multipole strengths were compared with predictions from consistent quasiparticle random phase approximation calculations. The theoretical predictions are in fair agreement with the experimental data. The  $E0$  strength was also compared with results from antisymmetrized molecular dynamics calculations found in the literature. A few peaks in the experimental data might be associated with clustering in  $^{24}\text{Mg}$ .

**Conclusions:** Ground-state deformation effects were observed in the isoscalar giant monopole resonance (ISGMR) and isoscalar giant quadrupole resonance (ISGQR) distributions. The ISGMR strength is split in two peaks around 19 and 28 MeV. The ISGQR exhibits a pronounced peak at 20 MeV with a broadening at the low-energy region, similar to predictions from microscopic calculations. Signatures of excitation of cluster states were observed in the  $E0$  response. Further studies including particle-decay measurements will be required to confirm the nature of the observed peaks.

DOI: [10.1103/PhysRevC.104.014607](https://doi.org/10.1103/PhysRevC.104.014607)

\*Present address: Department of Physics and Astronomy, Rowan University, Glassboro, NJ 08028, USA.

†Present address: Department of Physics and Astronomy, Dartmouth College, Hanover, NH 03755, USA.

‡Present address: Department of Physics and Astronomy, The University of North Carolina at Chapel Hill, NC 27599, USA.

§Present address: Institute of Modern Physics, Chinese Academy of Sciences, Lanzhou 730000, China.

## I. INTRODUCTION

Nuclear collective excitations are an important source of information about the structure and bulk properties of nuclei [1]. Compression modes like isoscalar giant monopole and dipole resonances are of particular interest because their energies are directly related to the nuclear-matter incompressibility [2–4] with significant consequences in many astrophysical phenomena [5].

Isoscalar giant resonances have been investigated for a large number of nuclei over the range  $Z = 6–92$  during the last decades [6–17]. Very interesting properties have been observed, such as overtone modes [18,19], off-shell nuclei softness [17,20], deformation effects [21,22], and many others. In particular, deformation effects in isoscalar giant resonances have recently been attracting a renewed interest due to the availability of fully consistent microscopic calculations and new experimental techniques that improve the sensitivity for the extraction of the resonance strengths, especially for light-mass nuclei. For instance, a splitting of the isoscalar giant monopole resonance (ISGMR) strength of  $^{24}\text{Mg}$ , due to its strong ground-state deformation, has recently been observed [23]. This effect can be understood as a mixing of the ISGMR with the  $K^\pi = 0^+$  component of the isoscalar giant quadrupole resonance (ISGQR) producing a two-peak structure in the ISGMR strength. In addition,  $^{24}\text{Mg}$  exhibits other interesting excitation modes such as cluster states that are expected to be present in  $N \approx Z$  light-mass nuclei [24]. For example, cluster states as  $^{20}\text{Ne} + \alpha$ ,  $^{12}\text{C} + ^{12}\text{C}$ , or  $^{16}\text{O} + 2\alpha$  configurations can be studied from the excited  $^{24}\text{Mg}$  nucleus. It has been proposed that cluster states are strongly populated by isoscalar monopole or dipole transitions [25–27]. Therefore, measurements with a good precision are required for identifying these states and the giant resonances simultaneously.

Inelastic scattering of  $\alpha$  particles at intermediate energies is a well-established technique that has been extensively employed in the investigation of isoscalar giant resonances for many years [6–17]. Alternatively, experiments using  $^6\text{Li}$  scattering have also proven to be a good method for investigating the isoscalar strength [28].  $^6\text{Li}$  experiments have an important advantage because of the better ratio between the resonance peak and the continuum [29]. As  $^6\text{Li}$  has a low particle emission threshold ( $S_\alpha = 1.47$  MeV), the breakup probability of the projectile is enhanced with the dominant channel  $d + \alpha$ . This reduces considerably the background component from the continuum and provides a better way to extract the strength up to high excitation energies.

In this work, the isoscalar giant resonances and a possible signature of clustering in  $^{24}\text{Mg}$  were investigated via  $^6\text{Li}$  scattering experiments. In combination with the favorable ratio of resonance-to-continuum background, the isoscalar  $E0$ ,  $E1$ , and  $E2$  transition strengths were reliably extracted. The experimental data were compared with previous  $\alpha$ -scattering experiments and with theoretical predictions to settle a discussion about deformation effects and clustering in  $^{24}\text{Mg}$ .

## II. EXPERIMENT

Measurements of inelastic scattering of  $^6\text{Li}$  particles were performed at the Research Center for Nuclear Physics (RCNP), Osaka University. The present data are part of a ( $^6\text{Li}$ ,  $^6\text{Li}' + \gamma$ ) experiment aiming to probe the isovector magnetic dipole transition strengths in the  $^6\text{Li}$  inelastic-scattering channel [30]. In this paper, we report about the singles ( $^6\text{Li}$ ,  $^6\text{Li}'$ ) data recorded during the experiment. Details of the experimental setup and procedure are explained in Refs. [28,30]. A brief description of the experiment is outlined below.

A 100-MeV/u  $^6\text{Li}$  beam was transported achromatically from the ring cyclotron to the Grand Raiden target position with an energy spread of 1.5 MeV in FWHM (full width at half-maximum). The beam intensity was monitored throughout the measurements and was approximately 1 pA. The target was a self-supporting 9.86-mg/cm<sup>2</sup>-thick foil of isotopically enriched (>99%)  $^{24}\text{Mg}$ . The Grand Raiden spectrometer [31], placed at 0° relative to the beam axis, was operated in the under-focus mode [32] to optimize simultaneously the angular resolutions in the dispersive [2.8-mrad (FWHM)] and nondispersive [10.3-mrad (FWHM)] planes. The unreacted beam was stopped in a 0° Faraday cup, which was placed at 12 m downstream of the focal plane [32]. The inelastically scattered  $^6\text{Li}$  particles were momentum-analyzed and identified by the focal-plane detection system. Two position-sensitive multiwire drift chambers (MWDCs) and three plastic scintillators were used for particle identification and reconstructing their trajectories [30]. By utilizing the positions from both MWDCs, the angles in the dispersive and nondispersive directions were determined. A calibration measurement was performed by using a sieve slit for the determination of the parameters of a ray-trace matrix for reconstructing the scattering angles at the target from position and angle measurements in the focal plane [33]. The momentum reconstruction of the  $^6\text{Li}$  ejectiles was calibrated by measuring the elastic-scattering peak from a  $^{93}\text{Nb}(^6\text{Li}, ^6\text{Li})$  reaction at several magnetic rigidities.

Three plastic scintillators in the focal plane (with thicknesses of 3, 10, and 10 mm) served to extract energy-loss signals and the time-of-flight that was measured relative to the radio-frequency signal of the AVF cyclotron. A 12-mm aluminum plate was placed in between the second and the third scintillators in order to improve the particle-identification capabilities.  $^6\text{Li}$  particles were stopped in this plate, whereas  $d$  and  $\alpha$  particles from  $^6\text{Li}$  breakup punched through and deposited energy in the third scintillator. Therefore, the signal from this detector was used as a veto to remove the contribution from  $^6\text{Li}$  breakup in the offline analysis. No instrumental background was present in the measurements around 0° scattering angle, and a subtraction through a parametrization of the instrumental background or through a side-band analysis was not necessary [28].

With the above Grand Raiden settings, inelastic scattering of  $^6\text{Li}$  particles at forward angles between  $\theta = 0^\circ$  and  $3^\circ$  was achieved. The magnetic-rigidity settings of the spectrometer

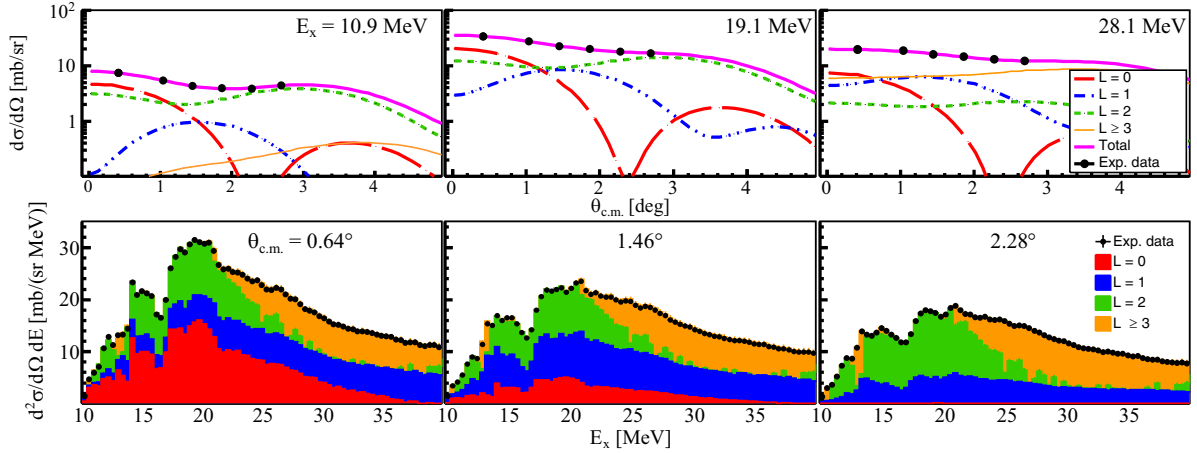


FIG. 1. On the top, angular distributions for the ( ${}^6\text{Li}$ ,  ${}^6\text{Li}'$ ) reaction on  ${}^{24}\text{Mg}$  at different excitation energies. The experimental data were fitted with MDA using DWBA calculations for angular-momentum transfers of  $\Delta L = 0-3$  (lines). On the bottom, double-differential cross sections for center-of-mass scattering angles at  $0.64^\circ$ ,  $1.46^\circ$ , and  $2.28^\circ$ . The stacked histograms show the MDA results for monopole (red), dipole (blue), quadrupole (green), and higher order (yellow) contributions.

covered excitation energies ( $E_x$ ) from 10 to 40 MeV. Absolute cross sections were determined on the basis of calibration runs in which the beam intensity was measured with a Faraday cup inserted before the reaction target in between runs. The normalizations from these calibration data were then applied to the other runs. The uncertainty in the absolute cross sections determined with this procedure was estimated at 20%, which was dominated by the read-out accuracy of the Faraday cup in the calibration runs due to the relatively low current.

### III. DATA ANALYSIS

Differential cross sections for inelastic scattering off  ${}^{24}\text{Mg}$  were obtained for angles between  $0^\circ$  and  $3^\circ$  in  $E_x$  intervals of 0.4 MeV. Figure 1(top) shows examples of angular distributions at selected energy regions. Double-differential cross sections of different multipolarities for energies between 10 to 40 MeV at certain angles are also presented in Fig. 1(bottom). These were determined via a multipole-decomposition analysis (MDA) [34], which was performed for each bin in  $E_x$  by fitting the differential cross section with a linear combination of distorted-wave Born approximation (DWBA) distributions for angular momentum transfers as

$$\left(\frac{d^2\sigma}{d\Omega dE}\right)^{\text{exp}} = \sum_L a_L(E_x) \left(\frac{d^2\sigma}{d\Omega dE}\right)^{\text{DWBA}}, \quad (1)$$

where  $a_L(E_x)$  is the fraction of energy-weighted sum rule (EWSR) for each multipole and the superscripts (exp and DWBA) denote the experimental and theoretical cross sections. These theoretical cross sections were obtained assuming 100% exhaustion of the EWSR for each multipole. The distorted wave Born approximation (DWBA) calculations were performed with the code CHUCK3 [35]. The transition potentials were obtained using a double-folding formalism with the M3Y-Paris nucleon-nucleon interaction [36]. A density-dependent term (BDM3Y1) was included to account for the reduction of the strength of the interaction as the density of

the medium increases [37]. The ground-state density distribution used in the folding analysis for  ${}^{24}\text{Mg}$  was taken from Ref. [38]. The resulting double-folding potential was used in the real and imaginary parts of the optical model (OM). The respective depths of the OM potential were adjusted to fit the elastic scattering data from Ref. [39]. The uncertainty due to the choice of the OM was estimated to be less than 6% in the different angular momentum components. The total systematic uncertainty in the multipole strengths was dominated by the MDA errors. Parametrizations for the transition densities, sum rules, and deformation factors employed in this analysis are described in Ref. [1].

Figure 1(top) shows the multipole components fitted to angular distributions at selected excitation energies. The stacked histograms (in colors) in Fig. 1(bottom) represent the contributions of each multipolarity extracted from the MDA. As can be seen, the monopole and quadrupole components have a significant contribution at the most forward angles. The  $L = 0$  strength is concentrated in the range from 10 to 40 MeV, while  $L = 2$  extends up to 30 MeV.  $L = 1$  and  $L \geq 3$  strengths are dominant mostly at the largest scattering angles measured and high-excitation energies.

### IV. RESULTS AND DISCUSSION

The strength distributions as fractions of the EWSRs for the different multipolarities were extracted from the fitted  $a_L(E_x)$  coefficients in the MDA with the following expressions [1,4]:

$$F_{S_0}(E_x) = \frac{2\hbar^2 A \langle r^2 \rangle}{mE_x} a_0(E_x), \quad (2)$$

$$F_{S_1}(E_x) = \frac{3\hbar^2 A}{32\pi mE_x} \left( 11 \langle r^4 \rangle - \frac{25}{3} \langle r^2 \rangle^2 - 10\epsilon \langle r^2 \rangle \right) a_1(E_x), \quad (3)$$

$$F_{S_{L \geq 2}}(E_x) = \frac{\hbar^2 A}{8\pi mE_x} L(L+1)^2 \langle r^{2L-2} \rangle a_L(E_x), \quad (4)$$

where  $m$ ,  $A$ , and  $\langle r^N \rangle$  are the nucleon mass, mass number and the  $N$ th moment of the ground-state density, respectively. The parameter  $\epsilon$  is obtained from the centroid-energy systematics of the ISGMR and ISGQR distributions [1] as  $\epsilon = (4/E_{\text{ISGQR}} + 5/E_{\text{ISGMR}})\hbar^2/3mA$ . Results of the monopole, dipole and quadrupole components are presented below.

### A. Monopole strength

The isoscalar  $E0$  strength of  $^{24}\text{Mg}$  has been measured in several experiments, including  $\alpha$  [23,40,41] and  $^6\text{Li}$  [29,39] inelastic scattering. However, the results of these experiments differ significantly in terms of the EWSR exhaustions and the shape of the strength distributions. For instance, the reported  $E0$  distributions exhibit a maximum value at different energies between 16 to 20 MeV, and their exhausted EWSRs vary from 57 to 106%. It is still not clear what the origin of these discrepancies is, in particular the large differences observed in previous  $^6\text{Li}$ -scattering experiments. A possible reason could be the method used for the instrumental and continuum background subtraction. The present data offer a new test for the isoscalar strength of  $^{24}\text{Mg}$ , with the advantage of an efficient background suppression provided by the experimental technique and the favorable resonance-to-continuum ratio of the  $^6\text{Li}$  probe.

The extracted ISGMR strength distribution in this experiment is shown in Fig. 2. The  $E0$  distribution exhausts  $51 \pm 5\%$  of the EWSR in the energy range 10–40 MeV. It is important to note that the energy resolution of this experiment is about 1.5-MeV FWHM. For comparison, the most recent results from  $\alpha$ -inelastic scattering experiments at TAMU (Texas A&M University) [41] and RCNP [23,42] are also plotted in the top panel of Fig. 2. The  $E0$  strength distribution obtained from the RCNP experiment exhausts  $57 \pm 7\%$  of the EWSR, which is consistent with our result. The  $E0$  strength distribution obtained from the TAMU experiment exhausts  $73 \pm 8\%$  of the EWSR in the same energy range. The excess of strength in the latter case could be associated with the parametrization employed for the background subtraction, as it has been observed in other experiments [43,44]. As can be seen, the shape of the  $E0$  distributions differ mostly in the energy range from 14 to 20 MeV. While the TAMU data have a broad distribution with strong components at 14, 17 and 19 and 22 MeV, the RCNP data exhibit a two-peak structure with centroids at 16 and 24 MeV. In fact, theoretical calculations predict that the ISGMR of  $^{24}\text{Mg}$  has a two-peak structure due to its large prolate ground-state deformation [23,45]. The  $E0$  strength extracted in this experiment shows a similar shape with two main components, a narrow peak located at  $E_x \sim 19$  MeV and a broad peak at  $E_x \sim 28$  MeV that extends up to high excitation energies. It is important to note that the position of the low energy peak in our experiment is 3 MeV higher than the value reported in Refs. [23,42] with the  $(\alpha, \alpha')$  RCNP data.

The extracted  $E0$  response was fitted by a superposition of five Lorentzian functions in the energy range from 10 to 40 MeV. In this case, the number of Lorentzians correspond to the same number of bumps observed in the data. The fitted parameters are presented in Table I. As can be noted,

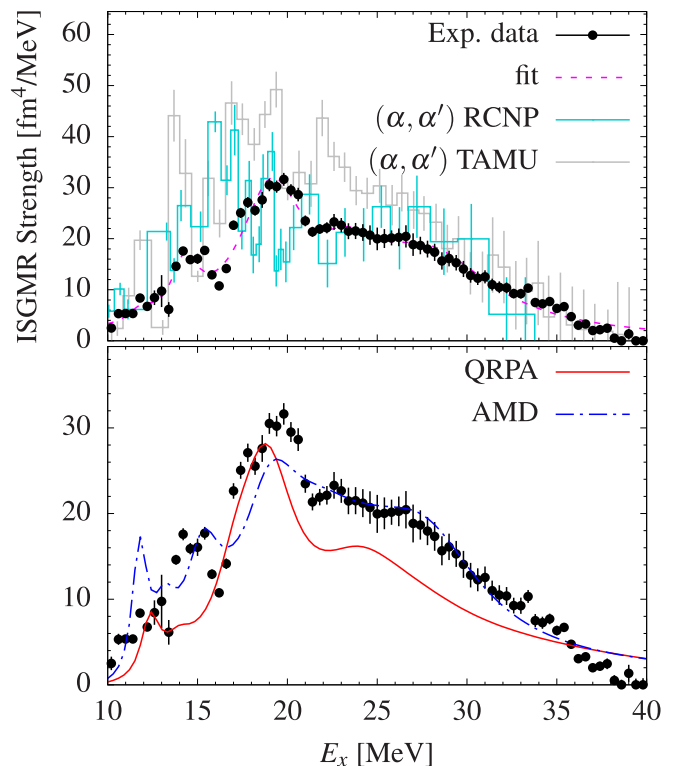


FIG. 2. ISGMR strength function. (Top) The experimental data are compared with results from  $\alpha$ -scattering experiments of Refs. [23,41] (bars). The data were fitted using a superposition of Lorentzian functions. (Bottom) Comparison with theoretical predictions from AMD [26] and fully consistent QRPA calculations. The QRPA distribution was shifted upward by 2 MeV.

the strength is exhausted mainly by two peaks [19.1(2) and 27.8(3) MeV] that are the principal components of the ISGMR, while other smaller contributions could be a signature of cluster vibrations in  $^{24}\text{Mg}$ . Antisymmetrized molecular dynamics (AMD) calculations predict the existence of molecular

TABLE I. Parameters of Lorentzian fits for the  $E0$ ,  $E1$ , and  $E2$  strength distributions of  $^{24}\text{Mg}$ .

$L[\hbar]$	$E_m$ [MeV]	$\Gamma$ [MeV]	EWSR [%]
0	$11.8 \pm 0.1$	$1.5 \pm 0.4$	$0.3 \pm 0.1$
	$14.3 \pm 0.1$	$1.7 \pm 0.4$	$2.0 \pm 0.5$
	$19.1 \pm 0.2$	$4.6 \pm 0.5$	$17.4 \pm 3.1$
	$23.4 \pm 0.3$	$4.4 \pm 0.9$	$6.5 \pm 1.5$
	$27.8 \pm 0.3$	$9.3 \pm 1.4$	$25.5 \pm 2.9$
1	$12.1 \pm 0.1$	$0.8 \pm 0.3$	$0.2 \pm 0.1$
	$13.5 \pm 0.1$	$0.9 \pm 0.2$	$2.3 \pm 0.7$
	$14.8 \pm 0.2$	$1.7 \pm 0.6$	$3.2 \pm 1.2$
	$17.9 \pm 0.1$	$1.8 \pm 0.5$	$5.8 \pm 2.4$
	$21.2 \pm 0.2$	$4.8 \pm 1.6$	$28.3 \pm 14.0$
	$26.1 \pm 0.3$	$6.0 \pm 2.5$	$45.3 \pm 20.4$
2	$11.4 \pm 0.1$	$0.9 \pm 0.2$	$2.0 \pm 0.6$
	$14.8 \pm 0.1$	$2.1 \pm 0.6$	$10.0 \pm 4.2$
	$18.4 \pm 0.4$	$3.6 \pm 1.1$	$26.5 \pm 10.7$
	$21.7 \pm 0.9$	$4.5 \pm 2.3$	$29.5 \pm 17.2$

states at energies near the cluster-decay thresholds [26,46]. For instance, in the case of  $^{24}\text{Mg}$ , molecular states such as  $^{20}\text{Ne} + \alpha$ ,  $^{12}\text{C} + ^{12}\text{C}$ , or  $n\alpha$  condensation are expected to be present in the isoscalar  $E0$  response. An AMD calculation for the isoscalar monopole strength of  $^{24}\text{Mg}$  was taken from Ref. [26]. This AMD calculation is plotted in the bottom part of Fig. 2. Here, the distribution was scaled by the respective EWSR ratio and folded with a Lorentzian function using an energy-dependent width [47]

$$\Delta(E') = \begin{cases} \Delta_0 & \text{for } E' \leq E_{\text{thr}} \\ \Delta_0 + a(E' - E_{\text{thr}}) & \text{for } E' > E_{\text{thr}} \end{cases} \quad (5)$$

to account for the energy spread and coupling to complex configurations that increase with the excitation energy. The parameters  $\Delta_0 = 0.1$  MeV,  $E_{\text{thr}} = 9.3$  MeV, and  $a = 0.38$  were chosen to reproduce the experimental strength distribution. The AMD  $0^+$  states at 9.3, 11.7, and 13.2 MeV have a large overlap between  $^{20}\text{Ne} + \alpha$ ,  $^{12}\text{C} + ^{12}\text{C}$ , and mean-field configurations [26]. In particular, the 11.7 MeV state seems to be consistent with the Lorentzian-peak fitted in the low-energy region. The peak at 14.3 MeV can be associated with a  $0^+$  state due to the  $^{12}\text{C} + ^{12}\text{C}$  configuration, which is predicted by the AMD calculations at 15.3 MeV. At higher excitation energies, AMD calculations also predict the existence of  $5\alpha$ -pentagon+ $\alpha$  cluster-states immersed in the ISGMR distribution [26]. A possible candidate for this exotic  $\alpha$ -cluster configuration is the peak at  $E_x = 23.4$  MeV, although further measurements including  $\alpha$ -decay data will be required to fully identify this state from the ISGMR mode.

The collective excitation modes in  $^{24}\text{Mg}$  were investigated within the microscopic mean-field-based quasiparticle random-phase approximation (QRPA). A consistent axially-symmetric-deformed Hartree-Fock-Bogoliubov (HFB) + QRPA approach using the DIM Gogny interaction [48,49], has been employed to calculate the  $L = 0, 1$ , and 2 strength distributions of  $^{24}\text{Mg}$ . Here, the single-particle wave functions are expanded in an optimized harmonic-oscillator basis with a large configuration space that included 15 major shells. In this case, the number of major shells employed is higher than the one used in Ref. [50] for the same nucleus. The new consideration allows for a better accuracy in the microscopic description of excited states in such a strongly deformed nucleus. In this approach, the intrinsic deformation of  $^{24}\text{Mg}$  ground state ( $\beta = 0.5$ ) was predicted by the HFB calculations as the minimum of the potential energy surface. The resulting model-space configuration allowed to build coherent two-quasiparticle (2-qp) excitations and the respective transition probabilities in the QRPA calculation. The ISGMR distribution from QRPA is shown in the bottom panel of Fig. 2. This distribution was scaled by the respective EWSR ratio and also folded with a Lorentzian function using the energy-dependent width of Eq. (5) with the same parameters. It is important to note that DIM + QRPA calculations for monopole and dipole strengths are systematically shifted by energies between 1 to 3 MeV with respect to the experimental distributions for a wide range of nuclei [28,51,52]. Therefore, the presently predicted QRPA energies were shifted (upward) by a constant factor of 2 MeV to account for a small energy displacement originating from the coupling between qp states

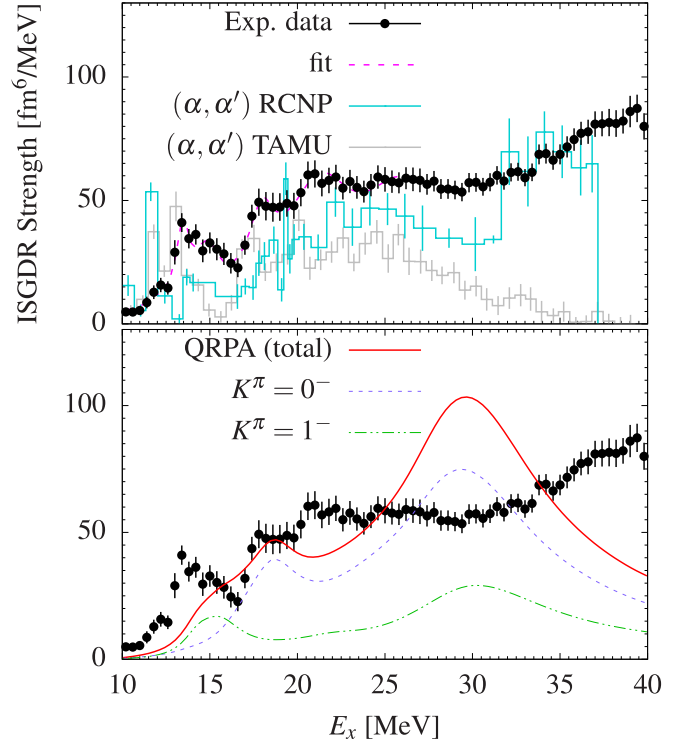


FIG. 3. ISGDR strength function. (Top) Same as Fig. 2. The data were fitted using a superposition of Lorentzian functions in the energy range from 10 to 26 MeV. (Bottom) Comparison with QRPA calculations showing the respective  $0^-$  and  $1^-$  components. The QRPA distributions were shifted upward by 2 MeV.

and phonons. As can be seen, the calculation is fairly consistent with the experimental data. The deformation effects lead to a double-peak distribution due to coupling to the  $K^\pi = 0^-$  component of the ISGQR. The same effect was investigated in Ref. [23] by comparing spherical and deformed QRPA calculations.

## B. Dipole strength

The  $E1$  response of  $^{24}\text{Mg}$  was also extracted from the MDA. Figure 3 shows the experimental distribution in the energy domain from 10 to 40 MeV. Due to the limited angular range covered in the experiment, the systematic uncertainties for excitation energies above 30 MeV are high and the separation between the  $L = 1$  and  $L \geq 3$  components becomes difficult (see Fig. 1). This  $E1$  distribution exhausts  $81 \pm 6\%$  of the EWSR in the energy range 10–30 MeV and  $188 \pm 29\%$  in the range 10–40 MeV. The distribution is also compared with results from  $(\alpha, \alpha')$  data measured at TAMU [41] and RCNP [42] [Fig. 3(top)]. The overall shape of the ISGDR (isoscalar giant dipole resonance) in the three distributions is similar up to 30 MeV, but the exhausted strength of the present data is about 22% to 38% higher than the  $(\alpha, \alpha')$  distributions in the same energy domain. It is important to mention that the continuum background was subtracted from the TAMU's data by using a background parametrization, whereas this procedure is not performed with the data measured at RCNP. The low energy region of the distri-

bution, below 16 MeV, contains a contribution from a few  $1^-$  states that were investigated in a recent work [53]. As shown in Table I, this region was fitted by three Lorentzian peaks centered at 12.1, 13.5, and 14.8 MeV. The strong 11.9 MeV (11% exhausted EWSR) reported in Ref. [53] was not observed in our data. This state seems to be inconsistent even with the  $(\alpha, \alpha')$  data from TAMU and RCNP experiments which exhaust about 2% of the EWSR at the same energy. However, the fitted peak at 13.5 MeV is consistent with the reported state  $1^-$  at 13.2 MeV in Ref. [53].

Cluster states in the isoscalar  $E1$  response are predicted to be populated by asymmetric configurations such as  $^{20}\text{Ne} + \alpha$  [27,54]. Therefore, the peaks at 12.1, 13.5, and 14.8 MeV (see Table I) are expected to carry part of this cluster configuration. The dipole strength increases beyond the energy of 26 MeV, but the results from  $\alpha$  inelastic scattering data exhibit a decreasing trend above this energy region. Therefore, the Lorentzian fitting was performed only up to the excitation energy of 26 MeV. The QRPA calculations are shown in Fig. 3(bottom). The QRPA strength was scaled by the EWSR ratio with the experimental data in the energy range 10–40 MeV. The same folding procedure of Eq. (5) was employed for this distribution. The  $0^-$  and  $1^-$  components are also plotted in the same figure. Both distributions were shifted by 2 MeV (upward), as it was performed for the  $L = 0$  calculation.

### C. Quadrupole strength

The ISGQR strength obtained from the MDA is presented in Fig. 4. The extracted  $E2$  response exhausts  $89 \pm 17\%$  of the EWSR in the energy range 10–40 MeV. The ISGQR strength obtained from  $\alpha$  inelastic scattering experiments at TAMU [41] and RCNP [42] are shown in Fig. 4(top). As can be seen, the three distributions have a similar shape up to 20 MeV. Above 20 MeV, the RCNP data exhibit a large strength over the other distributions, which might be caused by the continuum-background contribution. The ISGQR strength here presented has a pronounced peak that is consistent with the centroid energy  $64A^{-1/3}$  MeV from systematics [1].

Cluster-structure states are not easily correlated with the isoscalar quadrupole strength, sometimes the  $2^+$  band can be interpreted as  $^{20}\text{Ne} + \alpha$  configurations with a cluster-core excitation of  $^{20}\text{Ne}(2^+)$  [55]. Therefore, the peaks that were fitted in the  $E2$  strength distribution need to be investigated in finer detail to deduce evidence for a possible contribution from molecular configurations. A comparison with QRPA calculations is shown in the bottom part of Fig. 4. The present QRPA distributions were shifted by 2 MeV (upward), as it was done for the  $L = 0$  and  $L = 1$  calculations. The same folding procedure of Eq. (5) was employed for QRPA results. The  $K^\pi = 0^+, 1^+,$  and  $2^+$  components are also presented in the figure. The total QRPA strength is in good agreement with the experimental distribution. The strong ground-state deformation effects are clearly visible in the ISGQR strength that exhibits a broadening in the low-energy region due to the  $K^\pi = 0^+$  coupling with ISGMR states.

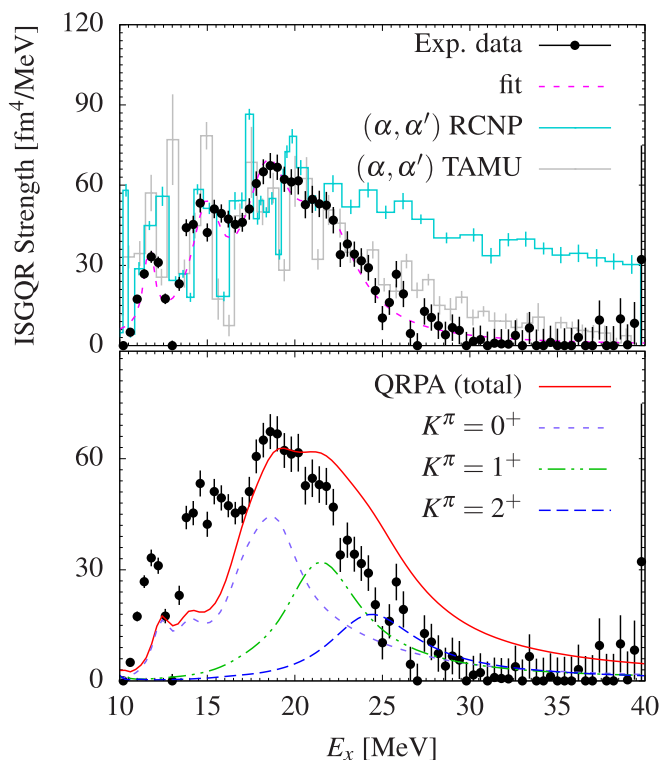


FIG. 4. ISGQR strength function. (Top) Same as Fig. 2. (Bottom) Comparison with QRPA calculations showing the respective  $K^\pi = 0^+, 1^+,$  and  $2^+$  components. The QRPA distributions were shifted upward by 2 MeV.

## V. SUMMARY

Inelastic scattering of  $^6\text{Li}$  particles at 100 MeV/u off  $^{24}\text{Mg}$  was measured at scattering angles between  $0^\circ$  and  $3^\circ$ . Measurements free of instrumental background and the very favorable resonance-to-continuum ratio of  $^6\text{Li}$  scattering enabled the precise extraction of the isoscalar  $E0$ ,  $E1$ , and  $E2$  strength distributions in  $^{24}\text{Mg}$ . A multipole-decomposition analysis was performed in the excitation-energy range from 10 to 40 MeV to extract the contributions from transitions associated with the transfer of different units of angular momentum. The obtained ISGMR distribution exhibit a two-peak structure, which can be explained by the strong deformation of the ground state of  $^{24}\text{Mg}$ . Due to the ISGMR  $K^\pi = 0^+$  coupling with the corresponding  $E2$  component, the ISGQR distribution also exhibits a broadening at the low-energy region. New ( $^6\text{Li}$ ,  $^6\text{Li}'$ ) measurements at larger scattering angles will be helpful to reduce the systematic uncertainties, in particular, for the higher  $L$  transfers.

State-of-the-art QRPA calculations are in fairly good agreement with the data and confirm the ground-state deformation effects. Additionally, a few other peaks were observed in the strength distributions. AMD calculations are also in good agreement with the data and suggest the existence of strong cluster states in the  $E0$  response that can be associated with the observed peaks. Further studies including particle-decay measurements will be required to confirm the nature of these resonances.

## ACKNOWLEDGMENTS

We thank the staff of RCNP for their tireless efforts in preparing the CAGRA array, the Grand Raiden spectrometer, and the  $^6\text{Li}$  beam. J.C.Z. thanks the support by Fundação de Amparo a Pesquisa do Estado de São Paulo (FAPESP) under Grants No. 2018/04965-4 and No. 2016/17612-7. This material was based on work supported by the National Science

Foundation under Grant No. PHY-1430152 (JINA Center for the Evolution of the Elements), PHY-1565546, PHY-1913554, PHY-1713857, and PHY-2011890, by the US DOE under Contract No. DE-AC02-06CH113567, by German BMBF Grant No. 05P19RDFN1, by the International Joint Research Promotion Program of Osaka University, by the DFG under Contract No. SFB 1245 (Project ID No. 279384907), and by the Hirose International Scholarship Foundation.

- 
- [1] M. N. Harakeh and A. van der Woude, *Giant Resonances: Fundamental High-Frequency Modes of Nuclear Excitation*, Oxford Science Publications (Oxford University Press, Oxford, 2001).
- [2] J. Blaziot, *Phys. Rep.* **64**, 171 (1980).
- [3] D. H. Youngblood, H. L. Clark, and Y.-W. Lui, *Phys. Rev. Lett.* **82**, 691 (1999).
- [4] U. Garg and G. Colò, *Prog. Part. Nucl. Phys.* **101**, 55 (2018).
- [5] M. Oertel, M. Hempel, T. Klähn, and S. Typel, *Rev. Mod. Phys.* **89**, 015007 (2017).
- [6] M. N. Harakeh, K. van der Borg, T. Ishimatsu, H. P. Morsch, A. van der Woude, and F. E. Bertrand, *Phys. Rev. Lett.* **38**, 676 (1977).
- [7] M. N. Harakeh, B. van Heyst, K. van der Borg, and A. van der Woude, *Nucl. Phys. A* **327**, 373 (1979).
- [8] J. van der Plicht, M. N. Harakeh, A. van der Woude, P. David, and J. Debrus, *Phys. Rev. Lett.* **42**, 1121 (1979).
- [9] M. N. Harakeh, H. P. Morsch, K. van der Weg, A. van der Woude, and F. E. Bertrand, *Phys. Rev. C* **21**, 768 (1980).
- [10] Y.-W. Lui, J. D. Bronson, C. M. Rozsa, D. H. Youngblood, P. Bogucki, and U. Garg, *Phys. Rev. C* **24**, 884 (1981).
- [11] H. J. Lu, S. Brandenburg, R. De Leo, M. N. Harakeh, T. D. Poelhekkens, and A. van der Woude, *Phys. Rev. C* **33**, 1116 (1986).
- [12] S. Brandenburg, R. De Leo, A. G. Drentje, M. N. Harakeh, H. Janszen, and A. van der Woude, *Phys. Rev. Lett.* **49**, 1687 (1982).
- [13] Y.-W. Lui, H. L. Clark, and D. H. Youngblood, *Phys. Rev. C* **64**, 064308 (2001).
- [14] B. John, Y. Tokimoto, Y.-W. Lui, H. L. Clark, X. Chen, and D. H. Youngblood, *Phys. Rev. C* **68**, 014305 (2003).
- [15] Y.-W. Lui, D. H. Youngblood, H. L. Clark, Y. Tokimoto, and B. John, *Phys. Rev. C* **73**, 014314 (2006).
- [16] T. Li *et al.*, *Phys. Rev. Lett.* **99**, 162503 (2007).
- [17] D. Patel *et al.*, *Phys. Lett. B* **718**, 447 (2012).
- [18] M. Hunyadi *et al.*, *Phys. Lett. B* **576**, 253 (2003).
- [19] H. L. Clark, Y.-W. Lui, and D. H. Youngblood, *Phys. Rev. C* **63**, 031301(R) (2001).
- [20] J. Piekarewicz, *Phys. Rev. C* **76**, 031301(R) (2007).
- [21] U. Garg, P. Bogucki, J. D. Bronson, Y. W. Lui, C. M. Rozsa, and D. H. Youngblood, *Phys. Rev. Lett.* **45**, 1670 (1980).
- [22] M. Itoh *et al.*, *Phys. Rev. C* **68**, 064602 (2003).
- [23] Y. K. Gupta *et al.*, *Phys. Lett. B* **748**, 343 (2015).
- [24] K. Ikeda, N. Takigawa, and H. Horiuchi, *Prog. Theor. Phys., Suppl.* **E68**, 464 (1968).
- [25] S. Lawitzki *et al.*, *Phys. Lett. B* **174**, 246 (1986).
- [26] Y. Chiba and M. Kimura, *Phys. Rev. C* **91**, 061302(R) (2015).
- [27] Y. Chiba, M. Kimura, and Y. Taniguchi, *Phys. Rev. C* **93**, 034319 (2016).
- [28] J. C. Zamora *et al.*, *Phys. Rev. C* **101**, 064609 (2020).
- [29] H. Dennert *et al.*, *Phys. Rev. C* **52**, 3195 (1995).
- [30] C. Sullivan *et al.*, *Phys. Rev. C* **98**, 015804 (2018).
- [31] M. Fujiwara *et al.*, *Nucl. Instrum. Methods Phys. Res. A* **422**, 484 (1999).
- [32] A. Tamii *et al.*, *Nucl. Instrum. Methods Phys. Res. A* **605**, 326 (2009).
- [33] C. J. Sullivan, Ph.D. thesis, Michigan State University, 2018.
- [34] B. Bonin *et al.*, *Nucl. Phys. A* **430**, 349 (1984).
- [35] P. D. Kunz, University of Colorado, 1978 (unpublished).
- [36] A. M. Kobos, B. A. Brown, R. Lindsay, and G. R. Satchler, *Nucl. Phys. A* **425**, 205 (1984).
- [37] D. T. Khoa and W. von Oertzen, *Phys. Lett. B* **342**, 6 (1995).
- [38] M. Pignanelli, S. Micheletti, R. De Leo, S. Brandenburg, and M. N. Harakeh, *Phys. Rev. C* **33**, 40 (1986).
- [39] X. Chen, Y. W. Lui, H. L. Clark, Y. Tokimoto, and D. H. Youngblood, *Phys. Rev. C* **80**, 014312 (2009).
- [40] D. H. Youngblood, Y.-W. Lui, and H. L. Clark, *Phys. Rev. C* **60**, 014304 (1999).
- [41] D. H. Youngblood, Y. W. Lui, X. F. Chen, and H. L. Clark, *Phys. Rev. C* **80**, 064318 (2009).
- [42] Y. K. Gupta *et al.*, *Phys. Rev. C* **93**, 044324 (2016).
- [43] D. H. Youngblood, Y. W. Lui, Krishichayan, J. Button, M. R. Anders, M. L. Gorelik, M. H. Urin, and S. Shlomo, *Phys. Rev. C* **88**, 021301(R) (2013).
- [44] Y. K. Gupta *et al.*, *Phys. Lett. B* **760**, 482 (2016).
- [45] J. Kvasil, V. Nesterenko, A. Repko, P.-G. Reinhard, and W. Kleinig, *EPJ Web Conf.* **107**, 05003 (2016).
- [46] M. Kimura, R. Yoshida, and M. Isaka, *Prog. Theor. Phys.* **127**, 287 (2012).
- [47] J. Kvasil, V. Nesterenko, W. Kleinig, D. Bozik, P.-G. Reinhard, and N. Lo Iudice, *Eur. Phys. J. A* **49**, 119 (2013).
- [48] S. Goriely, S. Hilaire, M. Girod, and S. Péru, *Phys. Rev. Lett.* **102**, 242501 (2009).
- [49] S. Péru and M. Martini, *Eur. Phys. J. A* **50**, 88 (2014).
- [50] S. Péru and H. Goutte, *Phys. Rev. C* **77**, 044313 (2008).
- [51] M. Martini, S. Péru, S. Hilaire, S. Goriely, and F. Lechaftois, *Phys. Rev. C* **94**, 014304 (2016).
- [52] S. Goriely, S. Hilaire, S. Péru, and K. Sieja, *Phys. Rev. C* **98**, 014327 (2018).
- [53] P. Adsley *et al.*, *Phys. Rev. C* **103**, 044315 (2021).
- [54] Y. Chiba, Y. Kanada-En'yo, and Y. Shikata, *Phys. Rev. C* **103**, 064311 (2021).
- [55] Y. Taniguchi, Y. Kanada-En'yo, and M. Kimura, *EPJ Web Conf.* **3**, 06004 (2010).